Slosh Dynamics in a Toroidal Tank

J. S. Meserole* and A. Fortini†
Boeing Aerospace Company, Seattle, Washington

An investigation is described of fluid slosh dynamics in a $\frac{1}{4}$-scale model of a toroidal liquid oxygen tank for a minimum-length orbit transfer vehicle. Experimentally and analytically derived equivalent mechanical models for the slosh modes under a 1-g acceleration are compared. Measurements of the reductions in slosh forces obtained with slosh baffles are presented, and equivalent mechanical models for the slosh modes with baffles installed are derived. A methodology is given for the efficient measurement of slosh dynamics by digital spectral analysis. Observations of nonlinear effects in the slosh motions are described.

Nomenclature

A = a factor in the annular tank solution
b = damping coefficient in equations of motion
C = Bessel function cross product
d = moment arm to vertical force sensors
f = horizontal force applied to tank
fz = vertical forces applied to tank
F = Laplace transform of f
g = acceleration due to gravity
h = height above tank bottom
h = without subscript: height of liquid surface
H = general second-order transfer function
j = square root of -1
J_1 = first-order Bessel function of the first kind
k = spring constant in equations of motion
k = without subscript: annular tank radius ratio
K = gain factor in H
L = length of pendulum flexures
m = mass
n = number of slosh modes
q = moment applied to the tank
Q = Laplace transform of q
r = minor radius of toroidal tank
R = major radius of toroidal tank
R_i, R_o = annular tank inner and outer radii
s = Laplace variable, $\sigma + j\omega$
T = tension in pendulum flexures
x = horizontal displacement
X = Laplace transform of x
Y_1 = first-order Bessel function of second kind
κ = a factor in the annular tank solution
ω = frequency, *rad/sec*
τ = time constant in H
ξ = zero of a Bessel function cross product
ζ = damping ratio

Subscripts

a = annular tank
c = center of mass of empty tank plus fixture
f = relating to force f
F = denotes a full tank
i = mode number
L = liquid contents of tank
p = pivot point of sway bars
T = denotes empty tank plus fixture

Presented as Paper 86-1717 at the AIAA/SAE/ASME/ASEE 22nd Joint Propulsion Conference, Huntsville, AL, June 16-18, 1986; received June 6, 1986; revision received Jan. 20, 1987. Copyright © American Institute of Aeronautics and Astronautics, Inc., 1987. All rights reserved..

*Principle Engineer, Propulsion Technology. Member AIAA.
†Principal Engineer, currently at Anthony Enterprises, Federal Way, WA. Member AIAA.

Introduction

THE designs of large satellites to be launched by the Space Transportation System (STS) will be often constrained not by STS weight limitations but by the limited volume of the STS payload bay. With such spacecraft, when additional orbit insertion propulsion is required, attachment to a compact orbit transfer stage would allow greater payload length or reduce the amount of space in the payload bay for which the user is charged. Current solid-fueled stages are relatively short; but for higher performance, greater payload, and on-orbit maneuvering, interest is growing in liquid bipropellant stages, and these are generally less compact. In particular, a reusable liquid hydrogen/liquid oxygen-fueled orbit transfer vehicle (OTV) for boosting large satellites to geosynchronous orbit must have a large volume for the low-density liquid hydrogen fuel.

A way of minimizing the length of a liquid-propellant stage is to carry one of the propellants (the liquid oxygen in the case of the OTV) in a toroidal tank and to nest the engine within the center of the tank. Such a configuration, however, poses difficulties in structural design and propellant management. A toroid is a flexible structure, and its large base area makes multiple outlets necessary for complete extraction of propellant. Furthermore, slosh dynamics in a toroid are much more difficult to predict than slosh dynamics in a cylinder or sphere.

This paper reports the results of an experimental investigation of slosh dynamics in a $\frac{1}{4}$-scale liquid oxygen toroidal tank for an STS-based OTV. The objective was to measure the slosh dynamics in a toroidal tank under 1-g acceleration and characterize them with equivalent linear mechanical (mass-spring-damper) models.[1] Such models are needed for the design of the vehicle attitude control system to ensure minimal dynamic interaction between the control system and the liquid propellant. Prior studies of toroidal tank slosh dynamics comprised measurements of slosh frequencies and forces in various model tanks and tank sections, but equivalent linear models were not obtained.[2-4]

A method of using modern digital data acquisition and modal analysis for determining linear slosh models was recently developed and applied to an investigation of slosh dynamics in a scale model of the ellipsoidal liquid oxygen tank for the Centaur G-Prime upper stage.[5] In the present study, digital data acquisition and analysis were also used, but the method chosen was a different one. In addition to the measurement of unobstructed sloshing in a toroidal tank, this

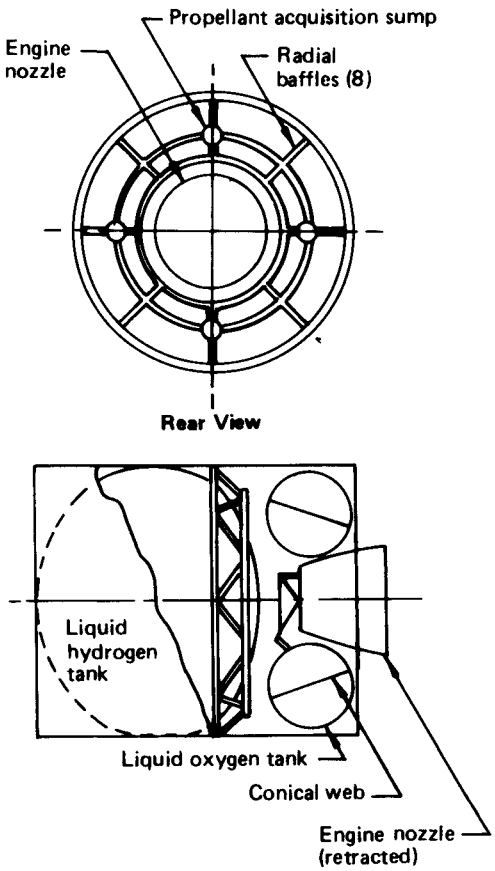

Fig. 1 OTV with a toroidal tank having an internal truss and baffles.

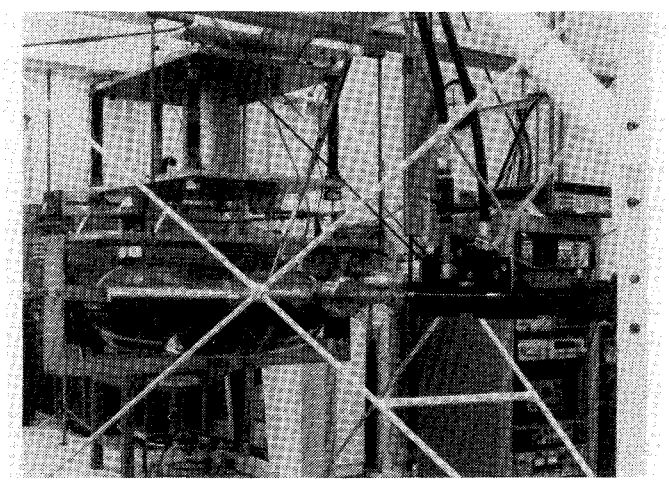

Fig. 2 Toroidal tank slosh measurement experiment apparatus.

study included measurements of the effectiveness of a baffle structure designed as a lightweight internal truss for stiffening the tank. Also, to compare to the experimental results, theoretical predictions for the parameters of the linear models for the slosh dynamics without baffles were derived using a conventional approach to approximating a toroidal tank by appropriately scaled annular cylindrical tanks,[1,3] for which an analytical solution to the fluid dynamics equations exists.[6]

One method of stiffening a toroidal tank and of preventing buckling at support attachment points without substantially increasing tank weight is to build in a truss structure comprising a circumferential cone and several radial bulkheads, as shown in Fig. 1. This particular truss configuration was derived on the basis of structural considerations, but it also provides two important nonstructural benefits. First, by segmenting the tank, it reduces the extent and force of fluid sloshing, and second, when the radial bulkheads are positioned over the tank outlets, they act as antivortex baffles and enable more rapid and complete draining of the tank.[7,8]

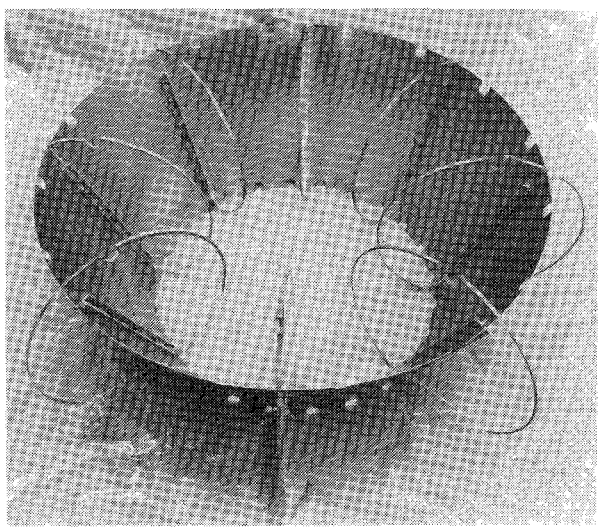

Fig. 3 Baffle structure used in the one-quarter-scale OTV toroidal tank.

Experiment Apparatus

Test Facility Hardware

The experiment facility constructed for the $\frac{1}{4}$-scale toroidal tank slosh measurements is shown in Fig. 2. It comprised a 0.94-m diameter toroidal tank made of transparent plastic and mounted on an aluminum fixture suspended by four steel flexures from an I-beam frame. These flexures constrained the horizontal motion of the tank to a single direction and kept the tank level. A hydraulic actuator moved it in accordance with prescribed commands. The actuator was servo-controlled and could be commanded with random or single sinusoid inputs to excite the fluid slosh modes collectively or individually. The test fluid was colored water.

In the figure, the tank does not have the baffle structure installed. That structure consisted of a conical circumferential web and eight unperforated radial bulkheads (Fig. 3). Eight radial bulkheads were chosen because fewer than that would not sufficiently stiffen a full-scale tank. The optimum number may be greater, depending on the details of the tank and vehicle design. The bulkheads are load-carrying numbers, so they are unperforated to avoid stress concentrations. They have cut-outs at the bottom, however, for tank draining.

Instrumentation

Figure 2 also shows the locations of the load cells used to measure the horizontal and vertical forces exerted on the tank and fixture by the actuator and the vertical suspension. One sensor, mounted in the linkage between the actuator and the fixture, measured the horizontal forces in-line with the tank motion (side forces were not measured). Four other sensors mounted between the corners of the two plates at the top of the fixture measured the vertical forces so that the moments exerted on the tank could be determined. Sway bars (also mounted between the plates) reacted all the horizontal forces carried between the plates and up to the suspension flexures, leaving the vertical forces to be carried entirely through the sensors. Subtracting the sum of the vertical forces measured by the rear sensors from the sum of the two measurements from the front sensors yielded the reaction moment. A posi-

tion sensor contained in the actuator measured the motion of the tank.

Measurement data were recorded with a Hewlett Packard Model 5423A two-channel dynamics analyzer. The input to the first channel was always the measured displacement of the tank, whereas the input to the second channel was either the force or the moment measurement. The analyzer was capable of directly calculating (by cross correlation and Fourier transform) and storing, on tape, the transfer function relating the channel-two input to the channel-one input, so most of the data was recorded in that form. Thus, the data records were the complex-valued transfer functions (or, as they may be called in this case, the frequency response functions) giving the magnitude and phase of the system force and moment per unit of tank displacement, expressed as functions of excitation frequency.

An additional capability of the analyzer was the estimation of the second-order linear models that best fit the resonance peaks in the transfer functions. That is, it could determine by a least-squares curve-fitting algorithm the frequency, damping, and scale (size) of the analogous mass-spring-damper system that best represented each slosh resonance.

Experiment Procedure

At each of ten fluid levels in the tank, the actuator was driven briefly with a random input of bandwidth 0 to 4 Hz to excite all the slosh modes simultaneously (no measurable ones existed at frequencies above 4 Hz). The maximum excursion of the actuator was ± 5 mm. When the tank motion was stopped, the slosh motions were allowed to decay freely. The measurement interval was started at the commencement of the tank motion and continued through the decay period.

An alternate approach to determining the frequency response functions is to displace the tank with a purely sinusoidal motion at each of many frequencies within the frequency band of interest. After the slosh motion reaches steady state, measurements are taken of the ratios of the response force and moment to the tank displacement amplitude and of the phase differences between the responses and the displacement. However, when the damping ratio is as low as it is for fluid motion in a tank, this is a time-consuming process because transients are slow to decay, and data at or very near resonant frequencies are difficult to obtain because with continuous excitation the slosh motion grows large and becomes nonlinear. Also, any tank motion that deviates from a smooth sinusoid of a single frequency introduces errors. Using burst random excitation yielded the responses to all frequencies simultaneously and reduced the time required for the measurements, even though this approach requires averaging the data from repeated measurement intervals to obtain an accurate frequency response function. This approach also avoided any difficulty with imprecise tank motion.

Analytical Model and Parameter Identification

Using transfer function data for determining the parameter values that describe the fluid motion (i.e., the frequencies, amplitudes, and damping ratios) required that the mechanical model assumed for the fluid sloshing be defined and that the system equations of motion be written in frequency domain form (i.e., as transfer functions). Values for the parameters in those equations could then be determined by matching the individual terms of the equations to the terms of the generalized second-order transfer function used in the curve-fitting algorithm in the dynamics analyzer.

Linear Model

The assumptions made to derive a linearized model of the fluid-tank system were that (1) the pendulum motion of the tank was sufficiently small to be approximately linear, and (2) the fluid slosh dynamics could be represented by a summation of linear second-order models plus a rigid mass that moved as

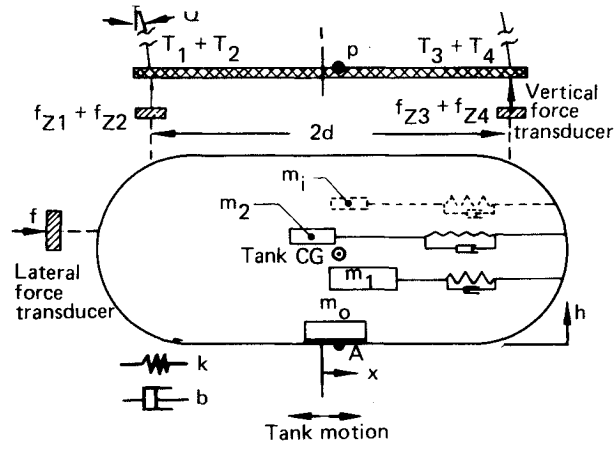

Fig. 4 Equivalent mechanical slosh model.

if fixed to the tank.[1,6] The resulting model is depicted schematically in Fig. 4.

Applying force and moment balances to this model system yields the following equations of motion:

Horizontal force balance

$$f = (m_T + m_o)\ddot{x}_o + b_o\dot{x}_o + \sum_{i=1}^{n}[b_i(\dot{x}_o - \dot{x}_i) + k_i(x_o - x_i)] + (T_1 + T_2 + T_3 + T_4)\sin\theta \quad (1)$$

Vertical force balance

$$(T_1 + T_2 + T_3 + T_4)\cos\theta = \left(m_T + m_o + \sum_{i=1}^{n} m_i\right)g \quad (2)$$

Force balance on slosh masses m_i

$$b_i(\dot{x}_o - \dot{x}_i) + k_i(x_0 - x_i) = m_i\ddot{x}_i \qquad i = 1,2,\ldots,n \quad (3)$$

Moment balance about point A

$$0 = [(f_{Z1} + f_{Z2}) - (f_{Z3} + f_{Z4})]d + fh_f - [m_T\ddot{x}_o h_c + m_o\ddot{x}_o h_o + b_o\dot{x}_o h_c + (T_1 + T_2 + T_3 + T_4)\sin\theta h_p] + \sum_{i=1}^{n}[b_i(\dot{x}_i - \dot{x}_o) + k_i(x_i - x_o)]h_i + \sum_{i=1}^{n} m_i g(x_i - x_o) \quad (4)$$

With θ small and with the substitution of Eqs. (2) and (3) into Eq. (1), the force balance becomes

$$f = \left[m_T\ddot{x}_o + b_o\dot{x}_o + m_T\frac{g}{L}x_o\right] + m_o\ddot{x}_o + \left(m_o + \sum_{i=1}^{n} m_i\right)\frac{g}{L}x_o + \sum_{i=1}^{n} m_i\ddot{x}_i \quad (5)$$

The measured horizontal force is f. The moment measured by the four vertical sensors is the first term in Eq. (4); let q be defined to be this quantity:

$$q = [(f_{Z1} + f_{Z2}) - (f_{Z3} + f_{Z4})]d \quad (6)$$

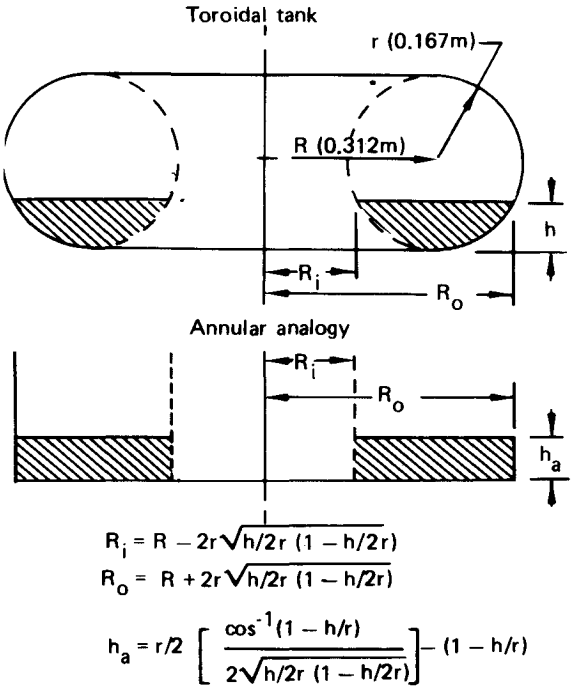

Fig. 5 Annular tank analogy used to obtain an approximate solution for the slosh modes in a toroidal tank.

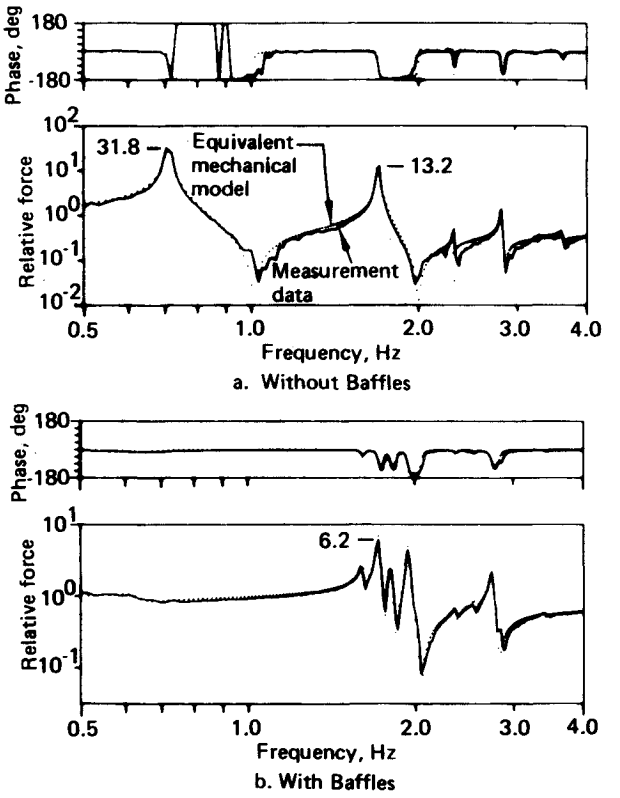

Fig. 6 Measured and modeled slosh force relative to force that would occur if the liquid were rigid. Tank fill ratio = 0.7.

Making the same substitutions in Eq. (4) as were made in Eq. (1) yields

$$q = -fh_f + m_T h_c \ddot{x}_o + m_o h_o \ddot{x}_o + b_o h_c \dot{x}_o + \left(m_T + m_o + \sum_{i=1}^{n} m_i\right)\frac{g}{L}h_p x_o + \sum_{i=1}^{n} m_i \ddot{x}_i h_i - \sum_{i=1}^{n} m_i g(x_i - x_o) \tag{7}$$

Substituting for f from Eq. (5) then gives

$$q = \left[m_T(h_c - h_f)\ddot{x}_o + b_o(h_c - h_f)\dot{x}_o + m_T\frac{g}{L}(h_p - h_f)x_o\right] + \left(m_o + \sum_{i=1}^{n} m_i\right)\frac{g}{L}(h_p - h_f)x_o + m_o(h_o - h_f)\ddot{x}_o + \sum_{i=1}^{n} m_i(h_f - h_i)\ddot{x}_i - \sum_{i=1}^{n} m_i g(x_i - x_o) \tag{8}$$

The transfer functions relating the force and the moment to the tank displacement are obtained by taking the Laplace transforms of Eqs. (5) and (8) (with all initial conditions zero) and then dividing by the displacement

$$\frac{F(s)}{X_o(s)} = \left[m_T s^2 + b_o s + m_T\frac{g}{L}\right] + \left(m_o + \sum_{i=1}^{n} m_i\right)\frac{g}{L} + m_o s^2 + \sum_{i=1}^{n} m_i s^2 \frac{X_i(s)}{X_o(s)} \tag{9}$$

$$\frac{Q(s)}{X_o(s)} = \left[m_T(h_c - h_f)s^2 + b_o(h_c - h_f)s + m_T\frac{g}{L}h_p\right] + \left(m_o + \sum_{i=1}^{n} m_i\right)\frac{g}{L}(h_p - h_f) + m_o(h_o - h_f)s^2 + \sum_{i=1}^{n} m_i(h_i - h_f)s^2\frac{X_i(s)}{X_o(s)} - \sum_{i=1}^{n} m_i g\left(\frac{X_i(s)}{X_o(s)} - 1\right) \tag{10}$$

The terms $X_i(s)/X_o(s)$ are eliminated by transforming Eq. (3) to obtain

$$\frac{X_i(s)}{X_o(s)} = \frac{b_i s + k_i}{m_i s^2 + b_i s + k_i} \qquad i = 1,2,\ldots,n \tag{11}$$

Also, the terms in square brackets that begin the right sides of Eqs. (9) and (10) are the force and moment transfer functions for the tank and its mounting fixture alone without liquid in the tank. They could each be directly measured without knowledge of their functional form. For simplicity, let them be denoted by

$$\left.\frac{F(s)}{X_o(s)}\right|_{\text{Tank}} \quad \text{and} \quad \left.\frac{Q(s)}{X_o(s)}\right|_{\text{Tank}}$$

Then, Eqs. (9) and (10) reduce to

$$\frac{F(s)}{X_o(s)} = \left.\frac{F(s)}{X_o(s)}\right|_{\text{Tank}} + m_L\frac{g}{L} + s^2\left[m_o + \sum_{i=1}^{n} m_i\frac{b_i s + k_i}{m_i s^2 + b_i s + k_i}\right] \tag{12}$$

$$\frac{Q(s)}{X_o(S)} = \frac{Q(s)}{X_o(s)}\bigg|_{\text{Tank}} + m_L\frac{g}{L}(h_p - h_f)$$
$$+s^2\left[m_o h_o(h_o - h_f)\right.$$
$$\left. + \sum_{i=1}^{n} m_i \frac{(b_i s + k_i)(h_i - h_f) + m_i g}{m_i s^2 + b_i s + k_i}\right] \quad (13)$$

where m_L is the total liquid mass

$$m_L = m_o + \sum_{i=1}^{n} m_i$$

The summation terms, which represent the fluid slosh dynamics, can be expressed in terms of the frequencies and damping ratios of the mass-spring-damper models, which are given by

$$\omega_i = \sqrt{k_i/m_i} \quad (14)$$

$$\zeta_i = (1/2\omega_i)\cdot(b_i/m_i) \quad (15)$$

Thus, Eqs. (12) and (13) can be written as

$$\frac{F(s)}{X_o(s)} = \frac{F(s)}{X_o(s)}\bigg|_{\text{Tank}} + m_L\frac{g}{L}$$
$$+s^2\left[m_o + \sum_{i=1}^{n} m_i \frac{2\zeta_i\omega_i s + \omega_i^2}{s^2 + 2\zeta_i\omega_i s + \omega_i^2}\right] \quad (16)$$

$$\frac{Q(s)}{X_o(s)} = \frac{Q(s)}{X_o(s)}\bigg|_{\text{Tank}} + m_L\frac{g}{L}(h_p - h_f)$$
$$+s^2\left\{m_o(h_o - h_f)\right.$$
$$\left. + \sum_{i=1}^{n} m_i(h_i - h_f)\frac{2\zeta_i\omega_i s + \left[\omega_i^2 + (g/h_i - h_f)\right]}{2^2 + 2\zeta_i\omega_i s + \omega_i^2}\right\} \quad (17)$$

The first terms in the equations represent, as noted previously, the forces and moments exerted by the tank and its fixture alone. The second terms give the added static restoring force and moment due to the liquid weight acting through the pendulum suspension. These were measured separately by making small, fixed tank displacements at each liquid fill level. The third terms describe the dynamic forces and moments due to liquid in the tank.

Data Reduction

Each of the transfer functions measured with the dynamics analyzer and recorded as complex-valued frequency response data was assumed to be modeled by Eqs. (16) and (17). (To put the equations in frequency response form like the data are, one sets the real part of the Laplace variable s to zero so that $s = j\omega$, where ω is the excitation frequency.) In reducing the data, the first step with each data record was to subtract the data record obtained with the tank empty. Then, the constant (independent of s) term due to the liquid weight, which was measured statically (i.e., with $s = j\omega = 0$), was subtracted. The result, represented by the entire third term in the model, was divided by $(j\omega)^2$ to eliminate the leading s^2 factor. Each resonance peak in the remaining data could then be assumed to be directly modeled by a single term in the summation. The resonant frequency, damping, slosh mass, and mass height of each of these slosh modes were then determined using the curve-fitting algorithm in the analyzer.

By a least-squares-error method, this algorithm determined values for the parameters ω, ζ, K, K_1, K_2, and τ in the linear second-order transfer function

$$H(s) = K\frac{\tau s + 1}{s^2 + 2\zeta\omega s + \omega^2} + K_1 + K_2 s \quad (18)$$

to obtain the best match to a resonance peak in the data. The factors K_1 and K_2 accounted for the presence of the other modes. The form of the leading term in Eq. (18) is identical to that of the terms in the summations in Eqs. (16) and (17); thus, for each resonance peak in the force and moment data, the values of ω_i, ζ_i, m_i and $(h_i - h_f)$ could be readily determined. Comparison of the denominators in the expressions yields $\omega_i = \omega$ and $\zeta_i = \zeta$, and when $\zeta \ll 1$ (as it always was), comparison of the numerators yields

$$m_i = \left(\frac{K}{\omega^2}\right)_{\text{force data}} \quad (19)$$

$$m_i(h_i - h_f)\left[1 + \frac{g}{\omega_i^2(h_i - h_f)}\right] = \left(\frac{K}{\omega^2}\right)_{\text{moment data}} \quad (20)$$

Then, since g is known and h_f is fixed by geometry, one can easily solve for h_i by using the fact that ω_i is necessarily the same in the force and moment data

$$h_i = h_f - \frac{g}{\omega_i^2} + \frac{K_{\text{force}}}{K_{\text{moment}}} \quad (21)$$

Annular Tank Analogy

The inviscid hydrodynamic equations for liquid sloshing in spherical, cylindrical, and cylindrical annular tanks have closed-form analytical solutions that can be used to predict the slosh modes in tanks of those shapes, but the equations for liquid sloshing in toroidal tanks do not have such a solution. An approximate one can be derived, however, from the solution for cylindrical annular tanks. An objective of the current investigation was to determine the accuracy of this approximate solution.

The solution is derived by approximating the toroidal tank with an annular tank in the way indicated in Fig. 5. With this approach, the surface dimensions of the liquid and the volume of the liquid are preserved in the transformation to the annular tank. For each fill level of the toroidal tank, the corresponding annular tank dimensions and fill level were used in the annular tank solution, which is expressible as an equivalent mechanical model comprising the frequencies, masses, and mass locations for the slosh modes. (The solution is for inviscid fluid motion, so it does not give damping ratios.) This approach is relevant only to sloshing in tanks without baffles.

The parameters of this analytically derived mechanical model of sloshing in an annular tank are given by

$$\omega_i = \sqrt{(g/R_o)\xi_i \tanh\kappa_i} \quad (22)$$

$$m_i = m_L\frac{A_i\left[(2/\pi\xi_i) - kC_i\right]\tanh\kappa_i}{(1 - k^2)\kappa_i} \quad (23)$$

$$h_{a_i} = h_a\left[1 - (2/\kappa_i)\tanh(\kappa_i/2)\right] \quad (24)$$

where

$$\kappa_i = (h_a/R_o)\xi_i \quad (25)$$

$$k = (R_i/R_o) \quad (26)$$

$$A_i = \frac{2[(2/\pi\xi_i) - kC_i]}{[(4/\pi^2\xi_i^2)](\xi_i^2 - 1) + C_i^2(1 - k\xi_i)^2} \quad (27)$$

$$C_i = J_1(k\xi_i)Y_1'(\xi_i) - J_1'(\xi_i)Y_1(k\xi_i) \quad (28)$$

and where J_1, Y_1 are the first-order Bessel functions of the first and second kind, respectively, J_1', Y_1' are the first derivatives of J_1 and Y_1, and ξ_i is the ith root of

$$J_1'(\xi_i)Y_1'(k\xi_i) - J_1'(k\xi_i)Y_1'(\xi_i) = 0 \quad (29)$$

(A table of the roots ξ_i as a function of k is given in Refs. 1 and 6.) Total liquid mass is denoted as m_L, and the height of center of slosh mass m_i above the tank bottom is denoted as h_{a_i}.

The mass heights h_{a_i} in the annular tank were transformed into corresponding heights h_i in the toroidal tank by equating fluid volumes contained beneath the levels h_{a_i} and h_i

$$h_{a_i} = \frac{r}{2}\left\{\frac{\cos^{-1}[1 - (h_i/r)]}{2\sqrt{(h_i/2r)[1 - (h_i/2r)]}} - [1 - (h_i/r)]\right\} \quad (30)$$

The values of h_i were solved for iteratively.

Results

A representative data record, reduced to show only the forces due to the liquid, is given in Fig. 6a. Shown plotted versus frequency is the force magnitude per unit of tank displacement divided by the force per unit displacement that would have been obtained had the liquid been rigid. These data were taken with the tank filled to $h/2r = 0.7$ without baffles installed. The figure shows six resonances, of which the first, second, and fourth have appreciable amplitudes.

Superimposed on the data is a dotted curve synthesized from the transfer function for the equivalent mechanical model created by summing six second-order models obtained from the data by the method previously described. The near congruence of the two curves demonstrates that curve-fitting to the frequency response data was an effective approach to determining the parameters for the equivalent mechanical model, and that the liquid motion was nearly linear under the low-amplitude random excitation used for the measurement. Complete quantitative results giving the model parameters at all fill levels are presented in a subsequent section.

Effect of Baffles

Figure 6b shows the slosh force frequency response obtained with baffles in the tank (again for the fill level 0.7). The baffles virtually eliminated the first mode and split the second mode into several less forceful ones. The baffle compartments were large enough that the fourth mode was not significantly affected, although its frequency was altered slightly. This portrays the effectiveness of the baffles in substantially reducing the amount of liquid mass that participates in any single slosh mode. At other fill levels, they were equally effective, as the data discussed in the following sections demonstrate.

To check the method of linear modeling on the data obtained with the baffles, the transfer function created by summing the second-order models derived from the data record in Fig. 6b was used to synthesize the dotted curve shown in the figure. Again, this curve lies closely on the measured curve, indicating that with the baffles the slosh motion was also predominantly linear under the excitation provided. This was true for all fill levels, with or without baffles installed.

Model Parameters

By the data reduction procedure described, the frequencies, masses, mass locations (height above the tank bottom), and damping ratios for equivalent mechanical models were determined for each of the fill levels at which data were taken.

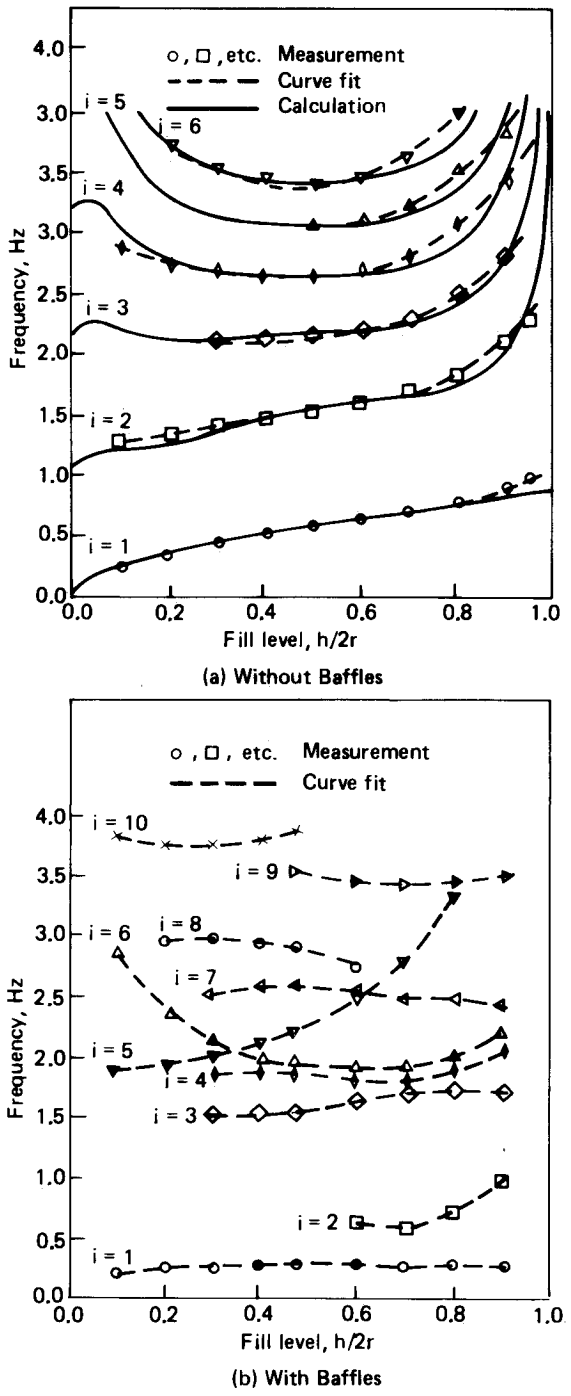

Fig. 7 Resonant frequencies of the slosh modes vs tank fill level.

Furthermore, Eqs. (22), (23), (24), and (30) were used to calculate estimates for the frequencies, masses, and mass locations, as functions of fill level, for the slosh motion without baffles. The complicated shapes of the internal compartments in the tank when baffles were installed precluded calculation of any estimates of the model parameters for that configuration.

The measured frequencies of the slosh modes without and with baffles are plotted versus tank fill level in Figs. 7a and 7b, respectively. The continuous curves in Fig. 7a represent the frequencies calculated using the annular tank analogy; the agreement for all six modes is close. In Fig. 7b, the dashed curves are smooth fits to the data. Some of the modes had measurable amplitudes only within a limited range of tank fill levels.

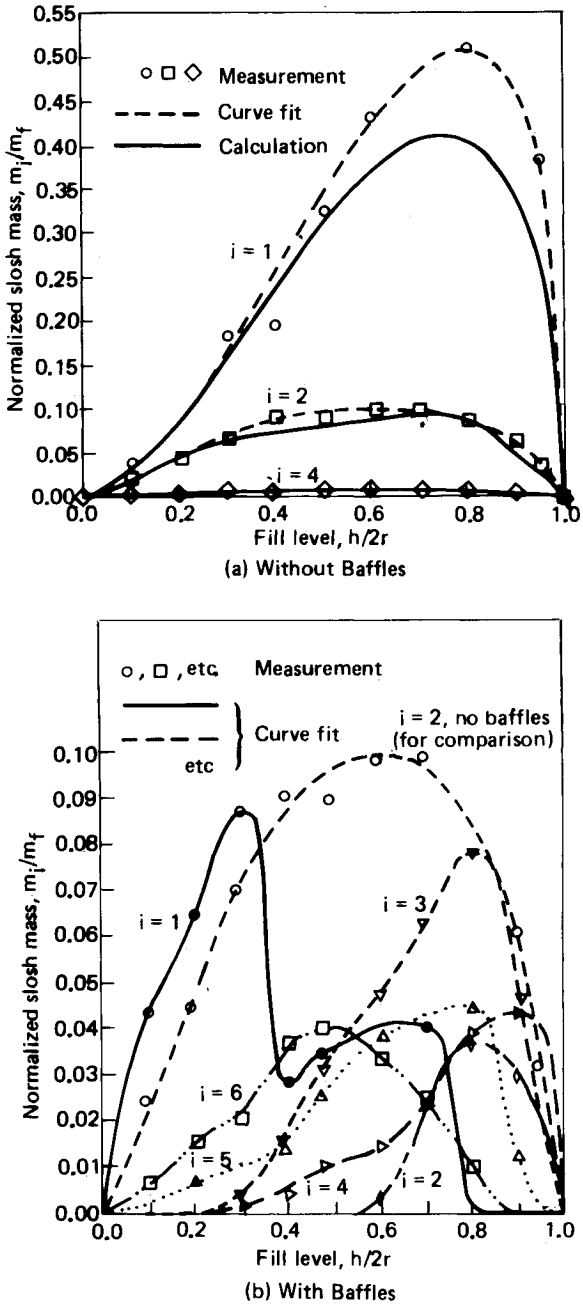

Fig. 8 Equivalent masses of the significant slosh modes.

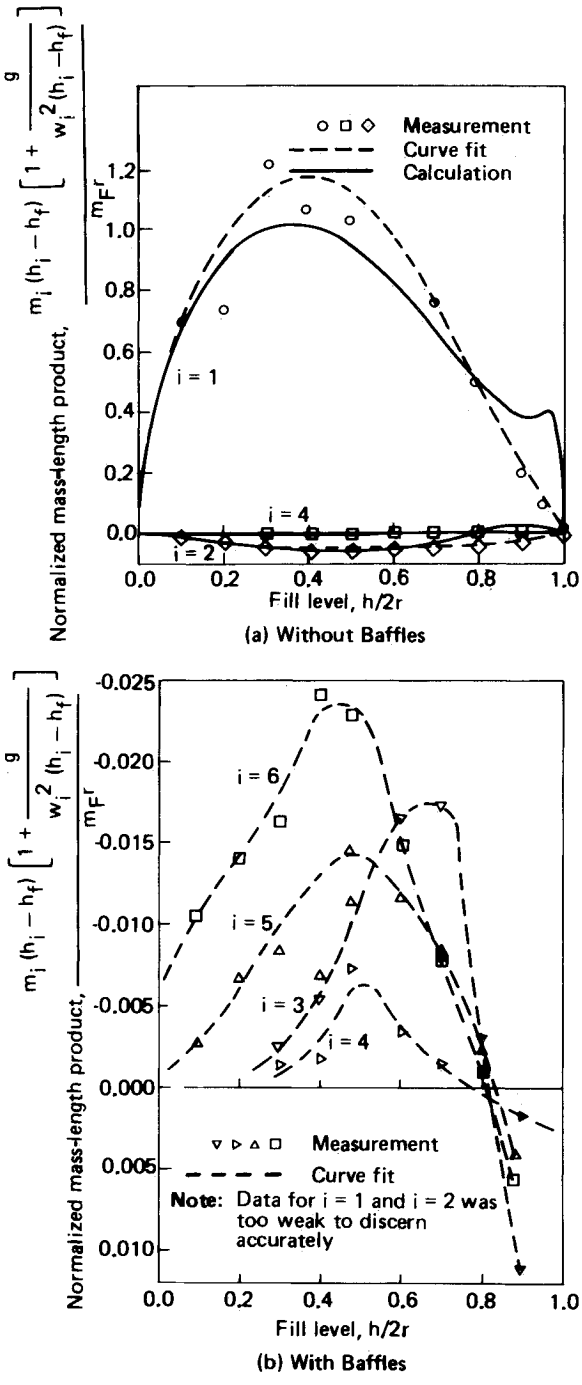

Fig. 9 Equivalent mass-length products.

The equivalent slosh masses m_i determined from the data for the three stronger slosh modes ($i = 1$, 2, and 4) that occur when there are no baffles are plotted in Fig. 8a. Here, the mass data have been normalized by the liquid mass m_F contained in the tank when full. Also given in the figure are curves calculated using the annular tank analogy. At the peak of the curve for the first mode, the calculated values for the model masses are 20% below the measured values. The discrepancy for the second mode is less, and for the fourth mode there is reasonable agreement. The probable reason the calculated values of the model masses are much less accurate than those of the frequencies, especially for the first mode at fill levels above 0.5, is that the shape and depth of the analogous annular tank inhibit more liquid from sloshing than do the curved and shallow sides of the toroidal tank. For the higher-order modes, this is a relatively less important factor, and the calculated values match the actual ones more accurately. For the calculation of resonant frequencies, on the other hand, the geometry of the fluid surface is much more important than the shape of the tank bottom, and because the annular tank analogy retains the toroidal tank liquid surface dimensions exactly, those calculations are accurate.

Figure 8b shows the model masses for the principal slosh modes when the baffles were installed. The mass data for the second mode when the baffles were not installed are replotted in this figure for comparison. This demonstrates the significant slosh mass reduction due to the baffles. The relative lack of effect on the first mode at the lowest fill levels results from the cut-outs at the bottom of the baffles for allowing liquid to flow to the tank outlets.

The mass data in Fig. 8 were obtained by reducing the force transfer function data and applying Eq. (19). Similarly, reduction of the moment data and use of Eq. (20) produced the data presented in Fig. 9. For purposes of description, those

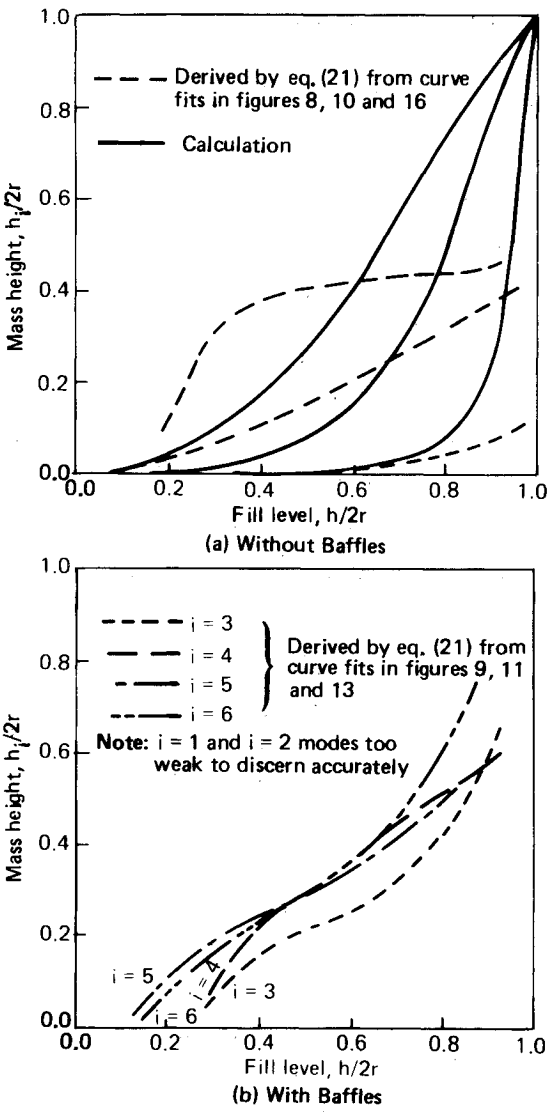

Fig. 10 Effective locations of the equivalent slosh masses.

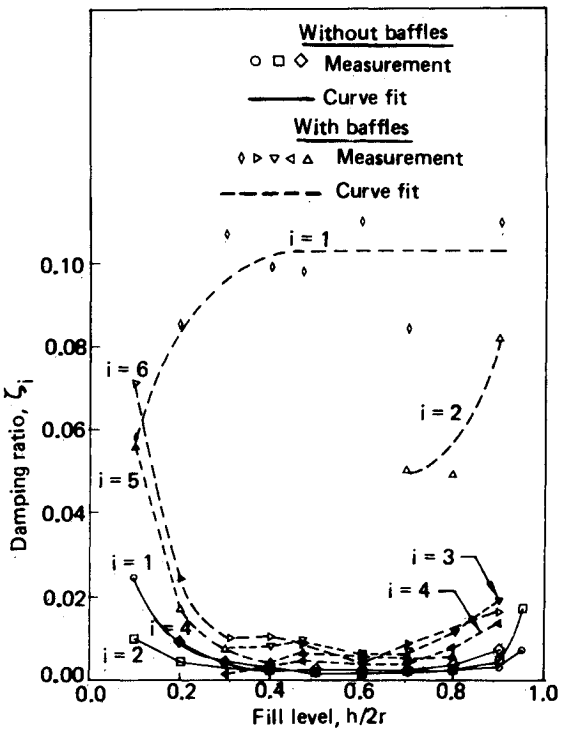

Fig. 11 Measured damping ratios—with and without baffles.

data have been termed the mass-length products for the slosh modes. In the figure, they have been normalized by m_F and r. Although these mass-length products are not directly required in the equivalent mechanical model, as the slosh masses are, these data have been plotted to enable fitting curves to them as was done with the mass data. The reason for fitting smooth curves to the data is that the calculation in Eq. (21) of the mass heights h_i is highly sensitive to scatter in the mass and mass-length data (and also in the frequency data when the frequency is low).

In Fig. 9a, the solid curves again show results calculated using the annular tank analogy. Similar to the slosh mass calculations, they underestimate the experiment data for the first mode. The peculiar hump in each curve, near $h/2r = 0.9$, is an artifact of the transformation that approximates the toroidal tank by annular ones.

Applying Eq. (21) to the smoothed data curves in Figs. 7–9 yields the curves in Fig. 10, which give the mass heights. Figure 10a also shows the curves calculated using the annular tank analogy. Again, the difference is substantial. In this case, though, the measured values appear unrealistic because they indicate that the sloshing liquid was far below the liquid surface. These values, however, were derived from the moment data using an assumed slosh model, and unmodeled vertical forces exerted by the sloshing liquid on the curved tank walls possibly produced moments that caused the assumed mass-spring models to appear lower in the tank than the sloshing liquid.

The measured damping ratios ζ_i are plotted in Fig. 11. Except the values for the first two modes with baffles, the damping ratios were consistently very low, ranging from about 0.002 without baffles to about 0.006 with baffles. (These values determined from the frequency response data were verified by independent measurements of the damping exhibited in free decay of the individual slosh modes.) Although the baffles do increase the damping, their major benefits are the large reduction in the liquid mass participating in the first mode and the splitting of the second mode into several smaller modes with separate reasonant frequencies.

Mode Shapes

After the frequency response data were obtained and the resonant frequencies identified, the tank (with the baffles removed) was oscillated at each of the no-baffles resonant frequencies for observation of the individual modes. Most of this was done at fill level 0.7, at which all six identified modes occurred. The mode shapes observed early in the oscillation are shown schematically in Fig. 12. With the exception of the transition from the first mode to the second, each increase in mode number adds a half wavelength within each of the circular cross sections.

Nonlinear Effects

When the oscillation was sustained, the simple lateral motion evolved in every case into a more complicated motion involving a wave (first mode) or waves (all other modes) traveling around the tank (Fig. 13). This rotary wave comprised fluid oscillation perpendicular to the excitation and so was a nonlinear effect. It would occur even with an excitation amplitude less than 1% of the outside diameter of the tank, provided that the excitation was sustained long enough. With all but the first mode, the rotary wave could not be excited independently of the lateral oscillation. With the highest modes, the result was a standing wave with a pattern of peaks and valleys, as shown in Fig. 13d.

For fill level 0.7, increasing the excitation frequency for the first mode to 0.74 from 0.71 Hz caused the planar (fixed nodal

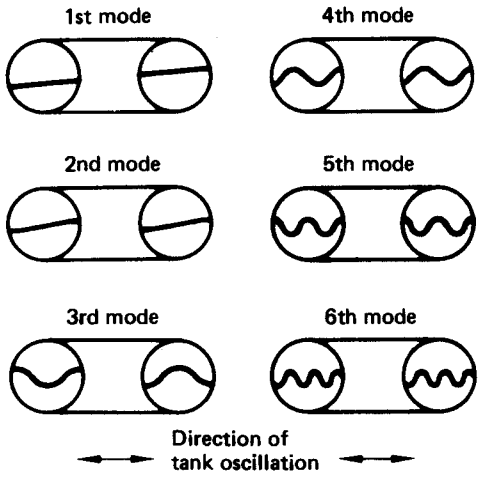

Fig. 12 Mode shapes of the lateral slosh resonances in a toroidal tank.

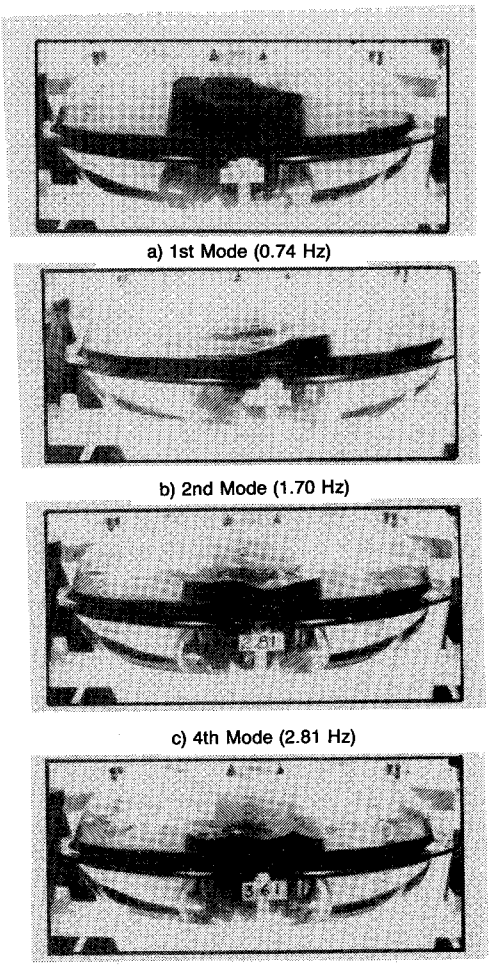

Fig. 13 End views of mode shapes after nonlinear transition to motion with rotary waves.

diameter) lateral motion to transition to the rotary wave (Fig. 13a), which was a stable nonplanar motion (the nodal diameter rotated at a steady rate). Decreasing the frequency back to 0.71 Hz caused the sloshing to revert to a purely lateral motion. This behavior is analogous to what occurs with a conical pendulum.[1] At low fill levels, though, the first mode transitioned into the rotary motion without requiring the slight increase in excitation frequency. It should be noted that the shape of the rotary mode was identical to that of the lateral mode; its distinguishing feature was its continuous circumferential motion. Thus, apparently it is the result of a summation of two equal but orthogonal transverse modes. This seems to be a plausible description of what occurs with the higher-order modes also, but the complex shapes that they evolve into suggest that perhaps a more complicated description is required.

Conclusion

Fluid slosh dynamics in a $\frac{1}{4}$-scale OTV toroidal tank undergoing lateral displacements were investigated experimentally to quantify the parameters in an equivalent mechanical model of the sloshing and to measure the effectiveness of slosh baffles in such a tank. The force and moment exerted on the tank by the liquid as functions of excitation frequency and tank fill level were measured, both with and without baffles installed in the tank, and a complete set of linear model parameters was obtained for each case by digital modal analysis. The results obtained for sloshing without baffles were compared to analytical estimates of the model parameters calculated by approximating the toroidal tank with cylindrical annular tanks and applying the solution of the hydrodynamic equations for annular tanks.

The experiment data verified that a structurally optimal design for internal stiffening members for toroidal tanks also is an excellent design for slosh baffles. Tests demonstrated that such baffles reduced the amount of liquid motion by 60%.

The approach developed for measuring the slosh dynamics and deriving equivalent mechanical models by digital modal analysis proved to be effective and accurate. Testing requirements were simplified, and even with the closely spaced slosh modes that occurred when the baffles were installed, the individual modes were readily distinguished and their parameters derived.

The frequencies of the toroidal tank slosh modes were accurately predicted by the adaptation of the analytical solution for slosh in an annular tank. On the other hand, the slosh masses and, hence, the peak slosh forces and moments were underpredicted substantially.

In certain circumstances, nonlinear effects were observed. It was found that continuous harmonic excitation of any single lateral slosh mode in a toroidal tank causes the lateral motion to evolve nonlinearly into a rotary mode involving waves traveling around the tank, analogous to what occurs with a conical pendulum.

References

[1]Abramson, H.N., ed., *The Dynamic Behavior of Liquids in Moving Containers*, NASA SP-106, 1966.

[2]McCarty, J.L., Leonard, H.W., and Walton, W.C. Jr., " Experimental Investigation of the Natural Frequencies of Liquids in Toroidal Tanks," NASA Tech. Note D-531, 1960.

[3]Sumner, I.E., "Preliminary Experimental Investigation of Frequencies and Forces Resulting From Liquid Sloshing in Toroidal Tanks," NASA Tech. Note D-1709, June 1963.

[4]Ketchum, W.J., "Orbit-to-Orbit Shuttle Toroidal Tank Outflow and Slosh Characteristics," AIAA Paper 70-1325, 1970.

[5]Unruh, J.F., Kana, D.D., Dodge, F.T., and Fey, T.A., "Digital Data Analysis Techniques for Extraction of Slosh Model Parameters," *Journal of Spacecraft and Rockets*, Vol. 23, March–April 1986, pp. 171–177.

[6]Roberts, J.R., Basurto, E.R., and Chen, P.Y., *Slosh Design Handbook*, NASA CR-406, May 1966.

[7]Fortini, A., "Vapor Pullthrough into Drains for a Rocket Engine Feedline from a Toroidal Tank," Boeing Aerospace Co., Seattle, WA, Document D180-28686-1, Feb. 1985.

[8]Fortini, A. and Wilson, A.C., "Vapor Pullthrough Control for an Abort Dump Outlet of a Toroidal Tank," Boeing Aerospace Co., Seattle, WA, Document D180-28685, Jan. 1985.